Journal of Materials Science & Technology 34 (2018) 112–118

Contents lists available at ScienceDirect

Journal of Materials Science & Technology

journal homepage: www.jmst.org

Fabrication of large-bulk ultrafine grained 6061 aluminum alloy by rolling and low-heat-input friction stir welding

C.Y. Liu[a,b], B. Qu[b], P. Xue[a], Z.Y. Ma[a,*], K. Luo[c], M.Z. Ma[d], R.P. Liu[d]

[a] Shenyang National Laboratory for Materials Science, Institute of Metal Research, Chinese Academy of Sciences, Shenyang 110016, China
[b] Key Laboratory of New Processing Technology for Nonferrous Metal & Materials, Ministry of Education, Guilin University of Technology, Guilin 541004, China
[c] Guangxi Key Laboratory of Universities for Clean Metallurgy and Comprehensive Utilization of Nonferrous Metal Resources, Guilin University of Technology, Guilin 541004, China
[d] State Key Laboratory of Metastable Materials Science and Technology, Yanshan University, Qinhuangdao 066004, China

ARTICLE INFO

Article history:
Received 11 September 2016
Received in revised form 10 January 2017
Accepted 10 January 2017
Available online 27 February 2017

Keywords:
Aluminum alloys
Ultrafine grained material
Friction stir welding
Mechanical properties

ABSTRACT

In this study, the ultrafine grained (UFG) 6061 Al alloys fabricated by cold rolling were friction stir welded (FSW) with different rotation rates under both air cooling and rapid cooling in water. Low-heat-input parameters of 400 rpm rotation rate in water (400-Water) could effectively inhibit the coarsening of recrystallized grains, reduce the precipitation rate, and retain more dislocations of the UFG 6061 Al parent metal. 400-Water joint showed high lowest-hardness value, narrow low-hardness zone, and high tensile strength, attributing to the effect of dislocation, grain boundary, solid-solution, and precipitation hardening. This work provides an effective strategy to fabricate large-sized bulk UFG Al alloy by cold rolling with large deformation and low-heat-input FSW.

1. Introduction

Ultrafine-grained (UFG) Al alloys fabricated by severe plastic deformation (SPD) have attracted great attention for structural applications because of their excellent mechanical properties and relatively simple preparation way of SPD [1–6]. Various SPD techniques including cryo-rolling (CR) [1], high-pressure torsion (HPT) [3], equal channel angular pressing (ECAP) [7], accumulative roll bonding (ARB) [8], and friction stir processing (FSP) [4–6], have been developed to produce UFG materials.

It should be noted that large bulk UFG Al alloys are hardly obtained using the current SPD technologies. For example, the size of UFG materials is severely restricted by the processing equipment during HPT and ECAP; and the inevitable edge cracking and fracture during ARB and CR greatly reduce the useful size. Therefore, the small size of UFG samples prepared by SPD becomes the key factor inhibiting the engineering applications.

In addition to the efforts of increasing the size of UFG samples via the optimization of mold design and processing parameters, welding SPD-fabricated UFG Al alloys is another effective method of increasing the size of UFG samples. However, the high temperature in conventional welding processes leads to severe coarsening of the ultrafine grains, which deteriorates the mechanical properties of the UFG Al alloys.

Friction stir welding (FSW), as an environment-friendly and energy-efficient "solid-state" joining technique, has been proven to be one of the most remarkable achievements in the welding field [9–18]. Similar to SPD technologies, FSW is also a plastic deformation process, and the grains of the parent metal (PM) can be refined during FSW [10,16–18]. Therefore, the fine grain structure and excellent mechanical properties of UFG Al alloys may be retained after FSW.

Sato et al. [19,20] first used FSW to weld the UFG Al fabricated by ECAP and ARB. Subsequently, UFG pure Al [21–24], UFG Al matrix composites [25], and UFG Al alloys [26,27] have been successfully welded by FSW. However, the strength of these welded samples is low [22,27]. For example, the UFG 1050 Al even shows lower hardness compared with its coarse grain counterpart after FSW [22]. The joint efficiency of the obtained FSW joints was found to be only 57% in the cold rolled Al-Mg-Sc-Zr alloy [27].

Heat is generated from severe friction between the rotation tool and the workpiece during plastic deformation of FSW. The maximum temperature in the stirred zone (SZ) usually reaches 400–480 °C [10]. Similar to other conventional welding processes,

* Corresponding author.
E-mail address: zyma@imr.ac.cn (Z.Y. Ma).

https://doi.org/10.1016/j.jmst.2017.02.008
1005-0302/

high heat input also leads to softening in the SZ [28]. Clearly, reducing the heat input during FSW is the key in producing large bulk UFG Al alloys with excellent mechanical properties.

In recent years, low rotation rate, high traverse speed, and additional rapid cooling have been proven effective in reducing heat input during FSW [13,29,30]. For example, liquid nitrogen, water, and dry ice have been used as cooling medium to decrease the peak temperature of Al alloys during FSW [10]. Xue et al. [13] found that the peak temperature and the duration at higher temperatures of the heat affected zone (HAZ) of pure Cu were significantly reduced when rapid cooling by flowing water and low rotation rate were applied during FSW. The temperature history of the SZ is very difficult to obtain during FSW, but the results of numerical analysis showed the peak temperature of the SZ decreased gradually when the cooling rate was increased [31].

In this study, UFG 6061 Al alloy produced by rolling with large deformation was friction stir welded with different rotation rates under both air cooling and rapid cooling in water. The aim of this work is to (a) obtain the large-sized bulk UFG Al alloy via SPD and FSW and (b) elucidate the influence of rapid cooling on the microstructure and mechanical properties of FSW joints of UFG 6061 Al alloy.

2. Experimental methods

The raw material was a cast ingot of commercially available 6061 Al alloy obtained from Alcoa Inc. The ingot was cut into samples with a dimension of 80 mm × 80 mm × 30 mm, solution-treated at 530 °C for 3 h, and then quenched in water. These solutionized samples were then rolled from 30 mm to 2 mm for 20 cycles at room temperature (the plastic strain is approximately 5.3) at a rolling speed of 0.4 m/s, obtaining UFG structure.

The rolled 6061 Al (UFG 6061 Al) were cut into Plates 300 mm in length and 70 mm in width, and were butt-welded along the rolling direction using an FSW machine under three conditions: (i) in air with an 800 rpm tool rotation rate (defined as 800-Air); (ii) in water with an 800 rpm tool rotation rate (defined as 800-Water); and (iii) in water with a 400 rpm tool rotation rate (defined as 400-Water). All FSW processes were performed at a constant traverse speed of 50 mm min^{-1}. A tool with a concave shoulder 10 mm in diameter and a taper threaded pin 1.7 mm in length was used. Fig. 1(a) shows the schematic illustration of the low-heat-input friction stir welding process.

The microstructures of the PM and the FSW samples were examined via transmission electron microscopy (TEM, JEM-2010). TEM images were obtained from the rolling direction–transverse direction (RD–TD) planes. The films for TEM were prepared by grinding to a thickness of 80 μm, followed by thinning using a twinjet electropolishing unit in a solution of 7 vol.% perchloric acid and 93 vol.% methanol at room temperature.

The Vickers hardness profiles were measured along the middle-thickness of the FSW samples perpendicular to the welding direction using a 200 g load for 10 s. Tensile tests were conducted on an Instron-5982-type testing machine at a strain rate of 1×10^{-4} s^{-1}. The tensile specimen with a gauge length of 21 mm was machined perpendicular to the welding direction (Fig. 1(b)). Fracture surfaces after the tensile tests were observed by scanning electron microscopy (SEM) to determine the failure mode.

3. Results

Fig. 2 shows the microstructure of the 6061 Al alloy after solid solution treatment and rolling with an equivalent strain of 5.3. Clearly, the UFG structure with an average grain size of 700 nm and ill-defined grain boundaries (GBs) was obtained in the rolled 6061 Al alloy. The UFG 6061 Al alloy was characterized by non-equilibrium GBs, high dislocation density, and absence of precipitates.

Fig. 3 shows the tensile properties of the UFG 6061 Al alloy tested along the TD direction. Sound properties of 0.2% yield strength (YS, ~380 MPa), ultimate strength (UTS, ~422 MPa), and elongation (EL, ~6%) were obtained in the initial UFG 6061 Al alloy.

Fig. 4 shows the Vickers hardness profiles across the SZ along the mid-thickness of the FSW UFG 6061 Al alloy joints under different welding parameters. The PM exhibited a high hardness value of ~125 HV. By comparison, the SZ of the FSW samples exhibited lower hardness, and the hardness value depended on the welding parameters. The average hardness value in the SZ of 800-Air was ~52 HV, which was only slightly higher than that of the as-annealed pure Al (40 HV [32]). However, the average hardness value in the SZ of 400-Water reached ~105 HV. This value was close to the hardness of the rolled UFG 6061 Al alloy. The highest hardness values of these welded samples appeared in the HAZ. The hardness value

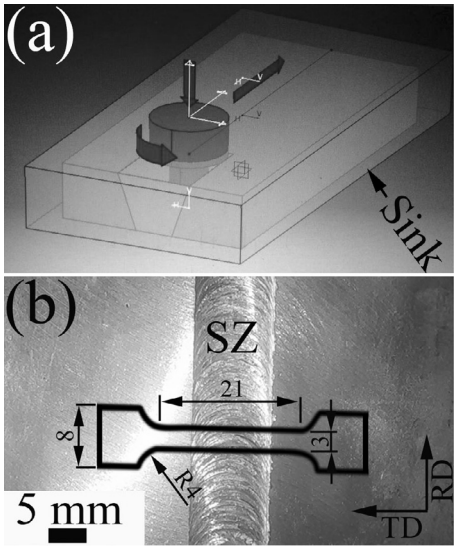

Fig. 1. (a) Schematic illustration of the low-heat-input friction stir welding process; and (b) dimension and location of the tensile specimen.

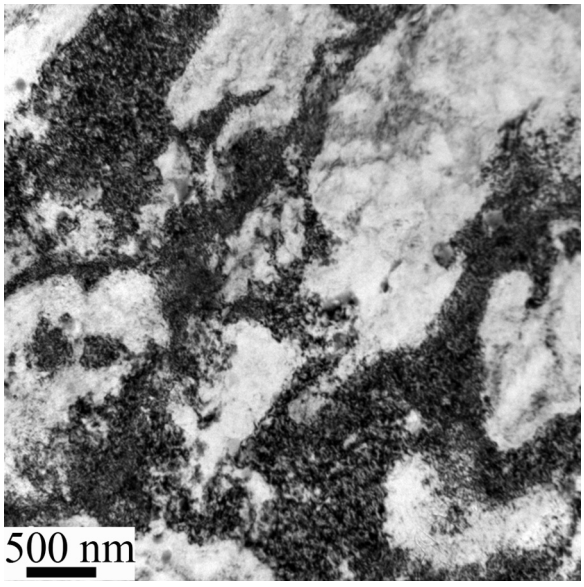

Fig. 2. TEM image of UFG 6061 Al alloy.

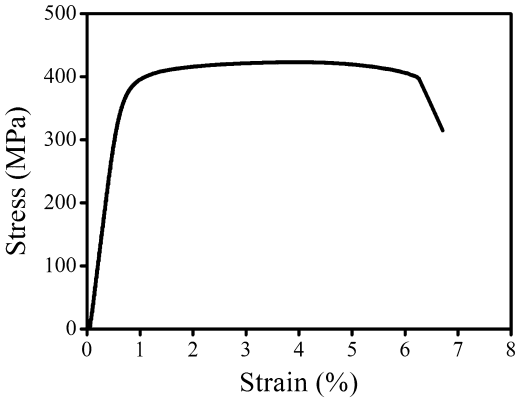

Fig. 3. Stress–strain curve of UFG 6061 Al alloy.

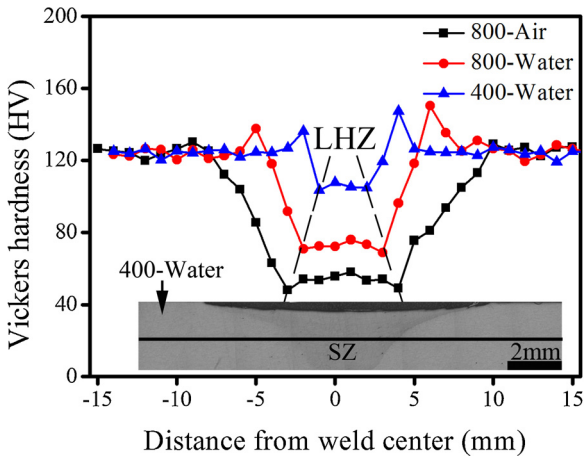

Fig. 4. Hardness profiles in cross-sections of FSW UFG 6061 Al joints at various parameters.

of 800-Water reached as high as 151 HV at the region 6 mm away from the centerline, where the HAZ is located. Compared with air cooling FSW joint, the water cooling joints showed narrowed low-hardness zone (LHZ) at both 800 and 400 rpm. In particular, the LHZ width of 400-Water decreased to 3 mm, which was close to that of stirring pin diameter.

Fig. 5 shows the TEM images of the SZ and HAZ of 800-Air. Equiaxed grains with sizes larger than 2 μm were observed in the SZ (Fig. 5(a)). The microstructure of the SZ was also characterized by low dislocation density and well-defined GBs. The equiaxed precipitates of ~200 nm were obtained in the SZ as shown in Fig. 5(b). Compared with the SZ, the HAZ exhibited smaller grains, slightly higher dislocation density, and slightly finer equiaxed precipitates (Fig. 5(c, d)). Furthermore, the rod-like precipitates with several tens of nanometers were observed in the HAZ as shown in Fig. 5(d).

Fig. 6 shows the TEM images of the SZ and HAZ of 800-Water. In the SZ, the equiaxed grains with sizes ~1 μm, and the equiaxed and rod-like precipitates with several or several tens of nanometers were obtained (Fig. 6(a, b)). In the HAZ, finer grains and higher dislocation density were observed (Fig. 6(c)). Furthermore, needle-like precipitates were also obtained in the HAZ as shown in Fig. 6(d).

Fig. 7 shows the TEM images of the SZ and HAZ of 400-Water. The SZ showed lower dislocation density compared with the rolled

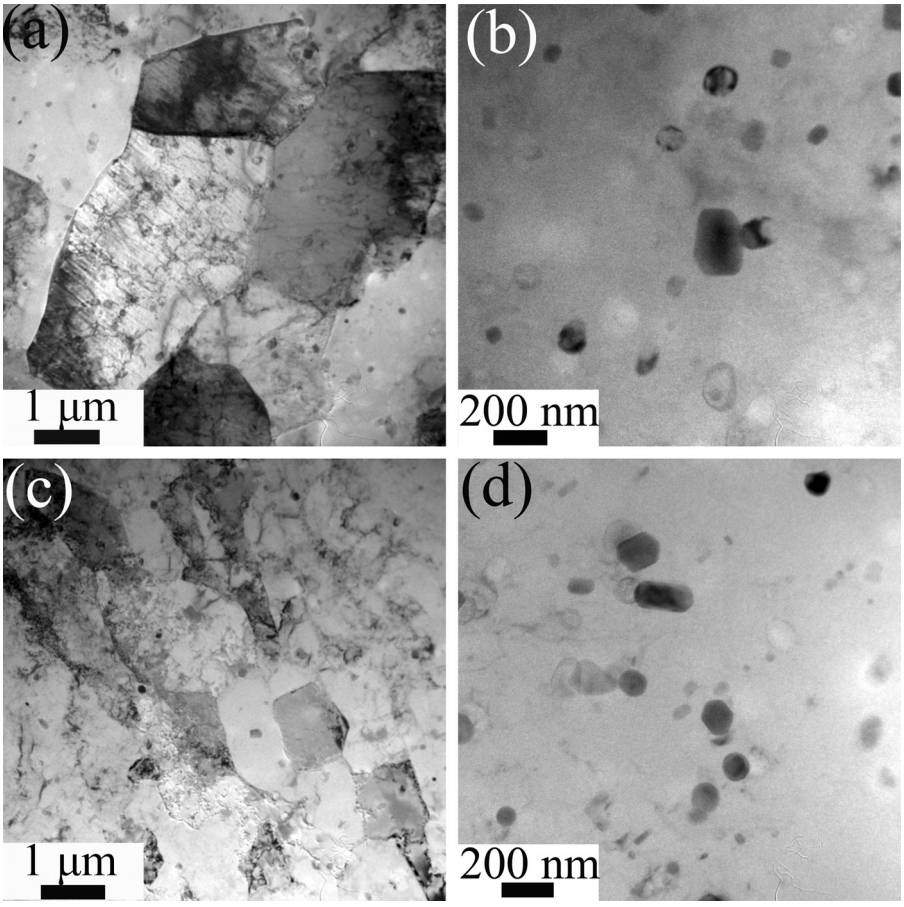

Fig. 5. TEM images of (a) and (b) SZ and (c) and (d) HAZ of 800-Air.

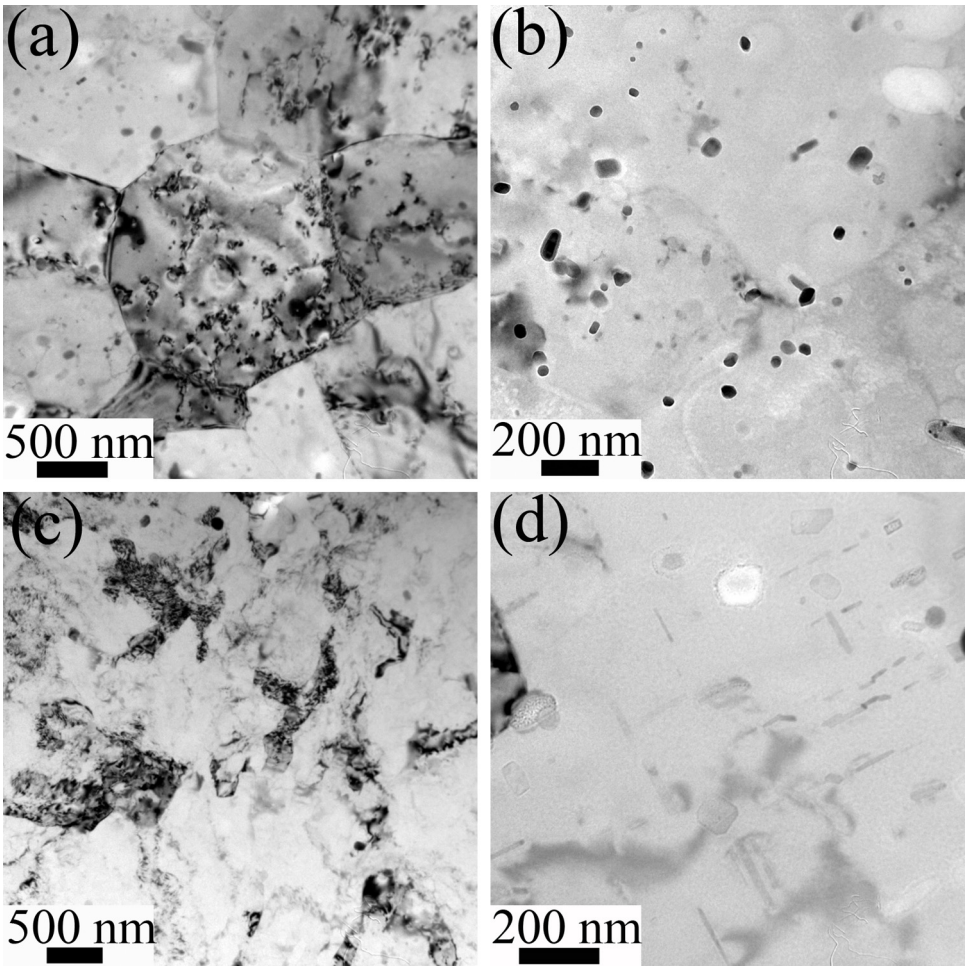

Fig. 6. TEM images of (a, b) SZ and (c, d) HAZ of 800-Water.

6061 Al alloy. The UFG structure with an average grain size of 300 nm was also obtained in this region as shown in Fig. 7(a). The equiaxed and rod-like precipitates of ~50 nm were observed in the SZ as shown in the TEM dark-field image (Fig. 7(b)). The HAZ exhibited a similar PM microstructure characterized by the UFG structure, non-equilibrium GBs, and high dislocation density (Fig. 7(c)). Furthermore, the precipitates with nanometer size were also obtained in the HAZ (Fig. 7(d)). Therefore, the large bulk UFG Al alloy was successfully fabricated via cold rolling with large deformation and FSW in water with a 400 rpm tool rotation rate.

Fig. 8 shows the stress–strain curves of the FSW samples. The samples welded in water showed a higher strength and lower ductility than the sample welded in air. 400-Water exhibited the highest YS and UTS of 276 and 308 MPa, respectively. The EL of 400-Water was 7.2%.

4. Discussion

The rolled 6061 Al alloy PM shows a typical SPD processed structure, i.e., UFG, high dislocation density, and non-equilibrium GBs after cold rolling with large deformation. The Si and Mg atoms in the 6061 Al alloy show high stability in the Al lattice during cold rolling; in addition, the dynamic precipitation found in other Al alloys [33,34] did not occur in this system. Therefore, the strengthening mechanism of the rolled UFG 6061 Al alloy includes boundary hardening by UFG, dislocation hardening, and solid-solution hardening by lattice distortion.

800-Air exhibited the lowest hardness in the SZ (Fig. 4). The high temperature present in the conventional FSW process led to coarsening of the UFG grains. Furthermore, the dislocation annihilation and the precipitation of the coarsened β phase occurred during FSW because of the high heat input (Fig. 5(a)). Therefore, the SZ showed the lowest hardness and the hardness increased with the distance from the SZ (Fig. 4). The HAZ even showed a higher hardness than that of the PM. This phenomenon can be attributed to precipitation hardening by heat-induced nanometer precipitates (Fig. 5(d)).

FSW in water can effectively inhibit the generation of a high temperature during processing [13]. The size of the recrystallized grains in the SZ was finer in 800-Water than in 800-Air. More dislocations were retained, and the precipitation rate obviously decreased (Fig. 6(a, b)). Consequently, the hardness value in the SZ of 800-Water improved. Compared with the PM, 800-Water showed a larger grain size and a lower dislocation density in the HAZ (Fig. 6(c)). However, the hardness in this area was significantly higher than that of the PM. This phenomenon can be attributed to the precipitation hardening effect. The metastable β″ phase which was characterized by needle-like shape and nanometer size was obtained in the HAZ of 800-Water (Fig. 6d). It is well known that the 6061 Al alloy achieves its optimal strength when the β″ phase precipitates from the Al matrix [33]. Therefore, the increase in the precipitation hardening effect overrides the loss of GB, dislocation, and solid-solution hardening effects in the HAZ of 800-Water.

TEM images (Fig. 7) indicate that a low heat input, which cannot led to the coarsening of recrystallization grain in the SZ, was achieved during the fabrication of 400-Water. The low heat input

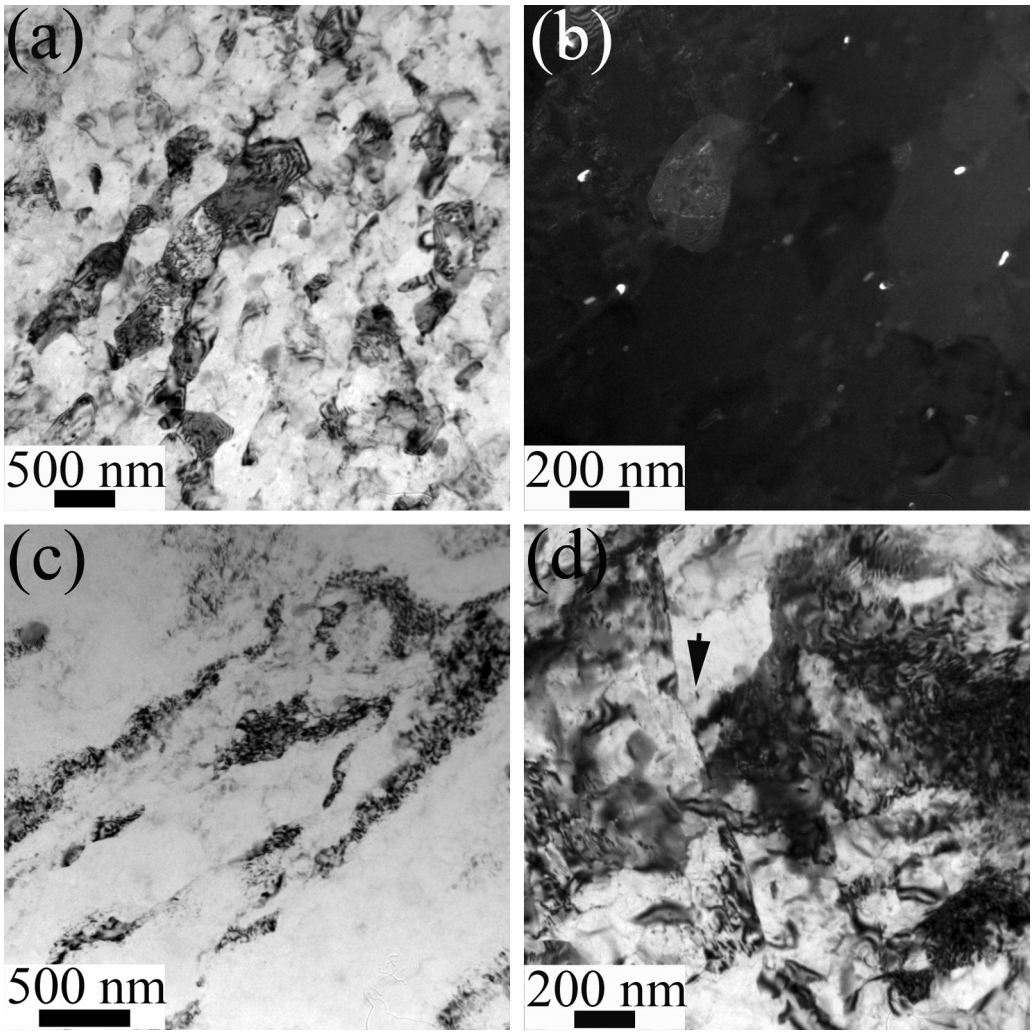

Fig. 7. TEM images of (a, b) SZ and (c, d) HAZ of 400-Water. Arrow in (d) denotes the precipitate.

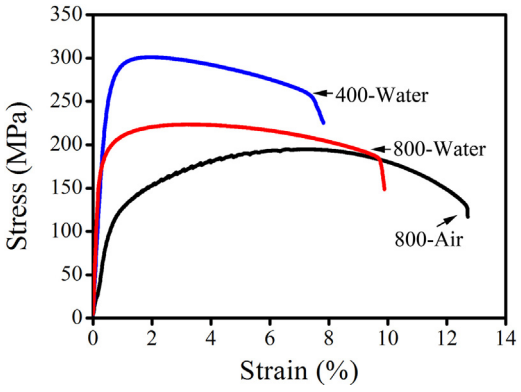

Fig. 8. Stress–strain curves of various FSW samples.

plays a significant role in determining the hardness of FSW joints [13,35,36]. Therefore, compared with other welding processes, FSW in water with 400 rpm can significantly enhanced the lowest-hardness value and decreased the LHZ width of FSW samples as shown in Fig. 4.

The precipitation was not inhibited during the fabrication of 400-Water (Fig. 7). A large number of crystalline defects, such as vacancies, dislocations, and GBs, were obtained in the UFG 6061 Al alloy because of the rolling deformation (Fig. 2). These crystalline defects provided a large number of atom propagation channels, which enhanced the mobility of the solute atoms during thermo-mechanical coupling [33,34,37,38]. Therefore, precipitation occurred in the UFG Al alloys under a low-heat-input FSW condition.

During tensile process, all of the FSW joints fractured at the SZ where the lowest-hardness value was observed in those joints as shown in Fig. 9(a). The YS, UTS, and EL of 800-Air were 115 MPa, 195 MPa, and 13%, respectively (Fig. 8). These mechanical properties of the present FSW joints of UFG 6061 Al alloy were similar to those of the FSW joints of conventional 6061-T6 Al alloy under similar welding parameters [39,40]. Therefore, the effect of the microstructure characteristics of the PM on the properties of the FSW joints of 6061 Al alloy was negligible during the conventional FSW process.

The YS, UTS, and EL of 800-Water were 188 MPa, 223 MPa, and 9.5%, respectively (Fig. 8). This sample shows much finer grains in the SZ, as compared with 800-Air (Fig. 5(a) and 6(a)). The finer grains led to a decrease in dislocation accumulation capability and an increase in GB hardening effect. So, compared with 800-Air, 800-Water shows higher strength, but lower work-hardening rate and EL value.

The tensile strength increased with further decreasing heat input in the FSW samples. 400-Water exhibits a joint efficiency of as high as 73%. Compared with the PM, the SZ of 400-Water exhibited smaller grains, lower dislocation density, and higher precipitate

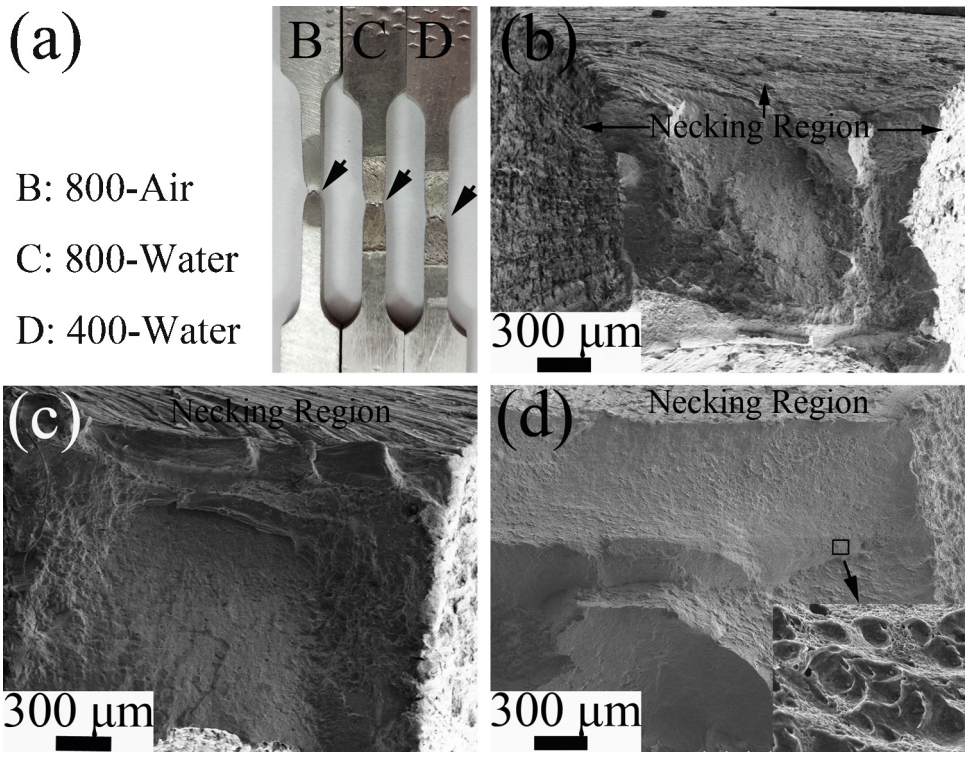

Fig. 9. (a) Fracture locations after the tensile test of various FSW samples; fracture surfaces after the tensile test of various FSW samples: (b) 800-Air, (c) 800-Water, and (d) 400-Water.

density (Fig. 7(a, b)). The decrease in dislocation hardening due to the annihilation of dislocations and solid solution strengthening due to the decomposition of solid solution is more pronounced than the increase in boundary hardening arising from grain refinement and precipitation strengthening caused by the precipitates. The net effect results in the decrease of UTS and YS after FSW in water with 400 rpm.

An SEM study of the fractured surfaces after the tensile tests was conducted to clarify the rupture mechanisms in the FSW samples (Fig. 9). The necking and dimples (the inset in Fig. 9(d)) in all samples exhibited a typical ductile fracture. So the FSW joints show well ductility.

5. Conclusions

This study suggests the potential of achieving large bulk UFG Al alloys using SPD and FSW. The following conclusions are reached:

(1) The UFG 6061 Al alloy could be fabricated by rolling with an equivalent strain of 5.3, which was characterized by non-equilibrium GBs, high dislocation density, absence of precipitates, and good mechanical properties.
(2) FSW in water could effectively inhibit the grain coarsening in recrystallization, retain the high dislocation density, and reduce the precipitation rate of the UFG 6061 Al alloy. Therefore, large bulk UFG 6061 Al alloys were successfully fabricated by cold rolling with large deformation and low-heat-input FSW.
(3) The samples welded in water showed high hardness and strength compared with that welded in air. A joint efficiency of 73% was obtained in 400-Water. The strengthening mechanism of 400-Water included dislocation, GB, solid-solution, and precipitation hardening. The FSW joints showed higher EL compared with that of the rolled 6061 Al alloy PM.

Acknowledgements

This work was funded by the National Natural Science Foundation of China (No. 51601045), the Guangxi Natural Science Foundation (No. 2015GXNSFBA139238), the Guangxi 'Bagui' Teams for Innovation and Research, the National Basic Research Program of China (No. 2013CB733000), and the Collaborative Innovation Center for Exploration of Hidden Nonferrous Metal Deposits and Development of New Materials in Guangxi.

References

[1] Y.H. Zhao, X.Z. Liao, S. Cheng, E. Ma, Y.T. Zhu, Adv. Mater. 18 (2006) 2280–2823.
[2] I. Sabirov, M.Y. Murashkin, R.Z. Valiev, Mater. Sci. Eng. A 560 (2013) 1–24.
[3] X. Sauvage, E.V. Bobruk, M.Y. Murashkin, Y. Nasedkina, N.A. Enikeev, R.Z. Valiev, Acta Mater. 98 (2015) 355–366.
[4] Z.Y. Ma, F.C. Liu, R.S. Mishra, Acta Mater. 58 (2010) 4693–4704.
[5] Z.Y. Ma, Metall. Mater. Trans. 39 (2008) 642–658.
[6] F.C. Liu, Z.Y. Ma, F.C. Zhang, J. Mater. Sci. Technol. 28 (2012) 1025–1030.
[7] M. Zha, Y.J. Li, R.H. Mathiesen, R. Bjørge, H.J. Roven, Mater. Sci. Eng. A 586 (2013) 374–381.
[8] X.X. Huang, Scripta Mater. 60 (2009) 1078–1082.
[9] W.M. Thomas, E.D., Nicholas, J.C., Needham, M.G., Murch, P., Templesmith, C.J., Dawes, G.B. Patent, No. 9125978, 1991, 8.
[10] R.S. Mishra, Z.Y. Ma, Mater. Sci. Eng. R 50 (2005) 1–78.
[11] R.Z. Xu, D.R. Ni, Q. Yang, C.Z. Liu, Z.Y. Ma, J. Mater. Sci. Technol. 32 (2016) 76–88.
[12] D. Wang, B.L. Xiao, Q.Z. Wang, Z.Y. Ma, J. Mater. Sci. Technol. 30 (2014) 54–60.
[13] P. Xue, B.L. Xiao, Q. Zhang, Z.Y. Ma, Scripta Mater. 64 (2011) 1051–1054.
[14] D. Wang, B.L. Xiao, D.R. Ni, Z.Y. Ma, Acta Metall. Sin. Engl. Lett. 27 (2014) 816–824.
[15] A.H. Feng, D.L. Chen, Z.Y. Ma, W.Y. Ma, R.J. Song, Acta Metall. Sin. Engl. Lett. 27 (2014) 723–729.
[16] Z.H. Zhang, W.Y. Li, Y. Feng, J.L. Li, Y.J. Chao, Acta Mater. 92 (2015) 117–125.
[17] F.F. Wang, W.Y. Li, J. Shen, S.Y. Hu, J.F. dos Santos, Mater. Des. 86 (2015) 933–940.
[18] Z.H. Zhang, W.Y. Li, J.L. Li, Y.J. Chao, A. Vairis, Mater. Charact. 107 (2015) 112–118.
[19] Y.S. Sato, M. Urata, H. Kokawa, K. Ikeda, Mater. Sci. Eng. A 354 (2003) 298–305.
[20] Y.S. Sato, Y. Kurihara, S.H.C. Park, H. Kokawa, N. Tsuji, Scripta Mater. 50 (2004) 57–60.

[21] I. Topic, H.W. Höpel, M. Göen, Mater. Sci. Eng. A 503 (2009) 163–166.
[22] Y.F. Sun, H. Fujii, Y. Takada, N. Tsuji, K. Nakata, K. Nogi, Mater. Sci. Eng. A 527 (2009) 317–321.
[23] M. SarkariKhorrami, M. Kazeminezhad, A.H. Kokabi, Mater. Des. 40 (2012) 364–372.
[24] M. Lipińska, L. Olejnik, A. Pietras, A. Rosochowski, P. Bazarnik, J. Goliński, T. Brynk, M. Lewandowsk, Mater. Des. 88 (2015) 22–31.
[25] M. Shamanian, M. Mohammadnezhad, J. Szpunar, J. Alloys Compd. 615 (2014) 651–656.
[26] I. Nikulin, S. Malopheyev, A. Kipelova, R. Kaibyshev, Mater. Lett. 66 (2012) 311–313.
[27] S. Malopheyev, S. Mironov, V. Kulitskiy, R. Kaibyshev, Mater. Sci. Eng. A 624 (2015) 132–139.
[28] Z.L. Liu, H.T. Cui, S.D. Ji, M.Q. Xu, X.C. Meng, J. Mater. Sci. Technol. 32 (2016) 1372–1377.
[29] Z. Zhang, B.L. Xiao, Z.Y. Ma, Mater. Charact. 106 (2015) 255–265.
[30] B.B. Wang, F.F. Chen, F. Liu, W.G. Wang, P. Xue, Z.Y. Ma, J. Mater. Sci. Technol. doi: http://dx.doi.org/10.1016/j.jmst.2017.01.016 in press.
[31] X.C. He, F.S. Gu, A. Ball, Prog. Mater. Sci. 65 (2014) 1–6.
[32] C.Y. Liu, B. Zhang, P.F. Yu, R. Jing, M.Z. Ma, R.P. Liu, Mater. Sci. Eng. A 580 (2013) 36–40.
[33] X. Sauvage, N. Enikeev, R. Valiev, Y. Nasedkina, M. Murashkin, Acta Mater. 72 (2014) 125–136.
[34] C.Y. Liu, L. Yu, M.Z. Ma, R.P. Liu, Z.Y. Ma, Philos. Mag. Lett. 95 (2015) 539–546.
[35] Z.H. Zhang, W.Y. Li, F.F. Wang, J.L. Li, Mater. Lett. 162 (2016) 94–96.
[36] Z.H. Zhang, W.Y. Li, Y. Feng, J.L. Li, Y.J. Chao, Mater. Sci. Eng. A 598 (2014) 312–318.
[37] X. Sauvage, E.V. Bobruk, M.Y. Murashkin, Y. Nasedkina, N.A. Enikeev, R.Z. Valiev, Acta Mater. 98 (2015) 355–366.
[38] G. Sha, K. Tugcu, X.Z. Liao, P.W. Trimby, M.Y. Murashkin, R.Z. Valiev, S.P. Ringer, Acta Mater. 63 (2014) 169–179.
[39] H.J. Liu, J.C. Hou, H. Guo, Mater. Des. 50 (2013) 872–878.
[40] L. Trueba Jr., G. Heredia, D. Rybicki, L.B. Johannes, J. Mater. Process. Technol. 219 (2015) 271–277.